KeAi

CHINESE ROOTS
GLOBAL IMPACT

### Contents lists available at ScienceDirect

### Petroleum Science

journal homepage: www.keaipublishing.com/en/journals/petroleum-science



### Original Paper

### Method for determining the installation interval of vortexing cuttings removal tool and its mechanism



Feng Chen <sup>a</sup>, Hong-Lin Lu <sup>a</sup>, Zhi-Hu Liu <sup>a</sup>, Wen-Chang Wang <sup>b,\*\*</sup>, Ya Liu <sup>c</sup>, Wei Wang <sup>c</sup>, Oin-Feng Di <sup>b,\*</sup>

- <sup>a</sup> School of Mechatronics Engineering and Automation, Shanghai University, Shanghai, 200072, China
- b Shanghai Institute of Applied Mathematics and Mechanics, School of Mechanics and Engineering Science, Shanghai University, Shanghai, 200072, China
- <sup>c</sup> Engineering Company, SINOPEC East China Oilfield Service Corporation, Yangzhou, 225100, Jiangsu, China

### ARTICLE INFO

# Article history: Received 25 July 2024 Received in revised form 20 February 2025 Accepted 7 August 2025 Available online 14 August 2025

Edited by Teng Zhu and Xi Zhang

Keywords:
Cuttings removal tool
Borehole cleaning
Installation positions
Computational fluid dynamics
Annular flow field

### ABSTRACT

Recent advancements in drilling technology have driven substantial progress in cuttings removal tool development, particularly for addressing borehole cleaning challenges in highly deviated directional critical factors in operational safety and efficiency improvement. Despite these innovations, two fundamental challenges persist: an incomplete understanding of mechanistic cuttings removal processes and an insufficient methodological framework for optimal tool installation. Studying the installation positions and assessing the effects of two cuttings removal are essential steps to advance the application of such tools. This investigation was initiated with a comprehensive analysis of particle settling dynamics and migration behaviors in annular wellbore spaces. Building upon Moore's terminal settling velocity equation, a modified model was developed to characterize the transport patterns of cuttings. Through model integration, the precise positioning of the efficient Vortex Cuttings Removal Tool (VCRT) was determined at 188 m from the bit. Subsequently, Computational Fluid Dynamics (CFD) numerical simulation was employed to reveal distinct annular flow field characteristics between VCRT and conventional drilling tools. Field validation in Well Z401X demonstrated a strong correlation between empirical measurements and simulated predictions, with pressure drop deviations of 6.25% and rotational speed variances limited to 7.50%. Analytical results confirmed VCRT's superior performance, exhibited 36.43% reductions in cuttings accumulation at the wellbore's lower quadrant compared to conventional drilling tools. The application of VCRT accelerated cuttings migration velocity in the annular space, significantly increasing the volume of returned onsite cuttings. Friction resistance decreased by approximately 35.90%, indicating higher cuttings removal efficiency than conventional drilling tools.

© 2025 The Authors. Publishing services by Elsevier B.V. on behalf of KeAi Communications Co. Ltd. This is an open access article under the CC BY-NC-ND license (http://creativecommons.org/licenses/by-nc-nd/4.0/).

### 1. Introduction

Many oilfields are situated in marginal zones with complex coastal and terrestrial conditions, which makes it challenging to meet the required production standards using vertical well technology (Mei, 2019; Jia et al., 2023). Conventional drilling and

Peer review under the responsibility of China University of Petroleum (Beijing).

production methods face inherent limitations. In contrast to vertical drilling, highly deviated wells offer distinct advantages, including extended horizontal reach, precise control over hydrocarbon reservoir drainage, and enhanced hydrocarbon recovery rates. Nevertheless, drilling such wells poses persistent technical challenges. Poor wellbore cleaning may induce various downhole operational risks (Andersen, 1998). The effectiveness of borehole cleaning is crucial for preventing non-productive time (NPT) incidents in drilling operations, including stuck-pipe incidents (Khan et al., 2021; Montes et al., 2024). Thus, maintaining efficient cuttings bed evacuation during the drilling of highly deviated and horizontal wells is imperative to ensure operational continuity.

<sup>\*</sup> Corresponding author.

<sup>\*\*</sup> Corresponding author.

E-mail addresses: wangwenchang 1982@163.com (W.-C. Wang), qinfengd@sina.com (Q.-F. Di).

F. Chen, H.-L. Lu, Z.-H. Liu et al. Petroleum Science 22 (2025) 3787–3802

The methods for removing cuttings bed accumulation can be broadly classified into two categories: drilling parameter optimization and the implementation of mechanical cuttings removal tools (Qu et al., 2017; Sayindla et al., 2017).

The primary adjustments to drilling parameters involve four critical operational dimensions: modification of drilling fluid rheological properties, regulation of annular return velocity, adaption of drill string rotational speed, and control of drill string eccentricity (Ozbayoglu et al., 2010; Pandya et al., 2020). Although hydraulic parameter optimization addresses cuttings bed challenges, this approach exhibits inherent limitations in field applications (Wang et al., 2013; Zuo et al., 2020; Li et al., 2022; Sun, 2023). Complementing parameter adjustment strategies, cuttings removal tools have proven indispensable in horizontal and highly deviated wells. A fundamental design principle mandates that the cleaning zone remains disengaged from borehole walls, interacting solely with drilling fluids or unconsolidated sediment layers (Boulet et al., 2000).

Current methodologies for determining tool placement primarily rely on empirical field data, resulting in substantial inconsistencies in installation protocols. This operational variability highlights the necessity for systematic investigation into optimal tool positioning. Technological advancements include the Cuttings Bed Impeller (CBI) developed by DBS researchers (Wylie et al., 2002; Rodman et al., 2003), which enhances removal efficiency when deployed at 152.4 m intervals along drill strings (Fig. 1(a)). Reinhardt et al. (2006) established standardized, specifically 1 heavy weight drill pipe or 4 drill pipes. The HydroClean series (Fig. 1 (b)) developed by VAM Van and Williams (2013) demonstrates superior cleaning performance with 2–3 pipe intervals (Van, 2013). Huang (2002) recommended every three drill pipes interval installations, while Zheng et al. (2018) designed the BH-HCS tool (Fig. 1(c)) with initial placement 120.82 m from the bit, significantly improving wellbore cleaning efficiency through field validation.

Zhang et al. (2017) devised a self-rotating cuttings removal tool (Fig. 2(a)) with an internal diversion mechanism. Analytical results demonstrate that the drilling fluid flow rate achieved by the self-rotating tool is approximately 1.4 times higher than that of the non-self-rotating tool, confirming its enhanced cuttings removal capability. Furthermore, Zhang et al. (2023 and 2024) analyzed a comparable turbine-structured self-rotating cuttings removal tool (Fig. 2(b)), demonstrating that the tool effectively reduces friction and performs well in inclined and short horizontal wells. Based on these findings, a similar tool was optimized by modifying the drive method for inclined tube-type split impeller turbine rotation.

Current research predominantly focuses on non-self-rotating cuttings removal tools, while self-rotating systems have received limited scholarly attention. Compared to rotary drilling, sliding drilling permits real-time directional adjustments guided by wellbore trajectory control. During this operation, the non-selfrotating tools become imperative for mitigating these operational constraints. In this context, the Vortexing Cuttings Removal Tool (VCRT) (Chen et al., 2022) is employed, featuring a turbine-like mechanism driven by drilling fluid flow during sliding operations. While existing studies have examined the removal mechanisms of VCRT (Chen et al., 2022), the optimal installation parameters remain undetermined. To address this gap, the methodology integrates three sequential phases. First, the cuttings settlingtransport behavior is analyzed through a modified Moore's terminal settling velocity equation, enabling predictive modeling of bed-prone annular sections. Second, VCRT installation is optimized via synthesis of the transport model, Z401X well trajectory data, and the structural characteristics of the drilling tool combination. Third, a CFD model of its flow field was constructed, and the cuttings removal effect under the action of the VCRT was

analyzed by numerical simulation. Finally, the VCRT was applied in the Z401X well to analyze the effect of cuttings removal under actual working conditions.

### 2. Determining the installation position of VCRT

### 2.1. Cuttings settlement and migration model

Cuttings migration in the horizontal wellbore primarily arises from solid-liquid coupling between the drilling fluid and cuttings particles. Cuttings and fluid flow characteristics are essential migration variables (Yu et al., 2023). The transport behavior of cuttings particles in the wellbore is a complex process, primarily influenced by two velocity components: the axial velocity component along the wellbore axis and the gravitational settling velocity component. The axial velocity component can be considered the same as the return velocity of drilling fluid in the annulus. Consequently, determining the settling velocity is crucial for accurately quantifying the displacement distances of cuttings particles in the wellbore.

The internal cuttings bed interaction characteristics between the fluid and cuttings particles are also crucial for understanding the entire hole cleaning process (Pedrosa et al., 2023). Individual cuttings particles in the wellbore experience four dominant forces along the direction of gravity: gravity, buoyancy, viscous drag, and pressure drag. Cuttings displacement along the direction of gravity is defined as settling motion. These force relationships acting on settling cuttings within the wellbore are graphically represented in Fig. 3 (Qu, 2021).

The movement of cuttings particles in drilling fluid is influenced by gravity and buoyancy. The difference between gravity and buoyancy is referred to as buoyant weight, and its expression is as follows:

$$F_{\rm B} = \frac{\pi d_{\rm S}^3}{6} (\rho_{\rm S} - \rho_{\rm I}) g \tag{1}$$

In Eq. (1):  $d_s$  represents the diameter of spherical cuttings particles, m;  $\rho_s$  represents the density of cuttings particles, kg/m³;  $\rho_l$  represents the density of drilling fluid, kg/m³; g represents the gravitational acceleration, m/s².

Due to the fluid's viscosity, cuttings particles are influenced by viscous drag during the settling process, with the direction of viscous drag opposing the direction of particle motion. When the settling velocity of cuttings particles is relatively high, separation phenomena occur on the particle surface (as shown in Fig. 3). This results in the formation of a pressure differential resistance on the particle surface, with the direction of pressure differential resistance being the same as the direction of particle motion. The combined force of pressure and viscous drag is termed viscous resistance, and its expression is as follows:

$$F_{\rm D} = C_{\rm D} \frac{\pi d_{\rm S}^2}{4} \frac{\rho_{\rm I} \nu^2}{2} \tag{2}$$

In Eq. (2):  $C_D$  represents the resistance coefficient, which is dimensionless; v represents the settling velocity of cuttings particles. m/s.

The equilibrium equation for cuttings particles settling in quiescent fluid is:

$$F_{\rm B} - F_{\rm D} = m_{\rm S} \frac{{\rm d}\nu}{{\rm d}t} \tag{3}$$

In Eq. (3),  $m_s$  represents the mass of cuttings particles, kg. During the settling process of cuttings particles, the magnitude of viscous resistance  $F_D$  is directly proportional to  $v^2$ . In the initial

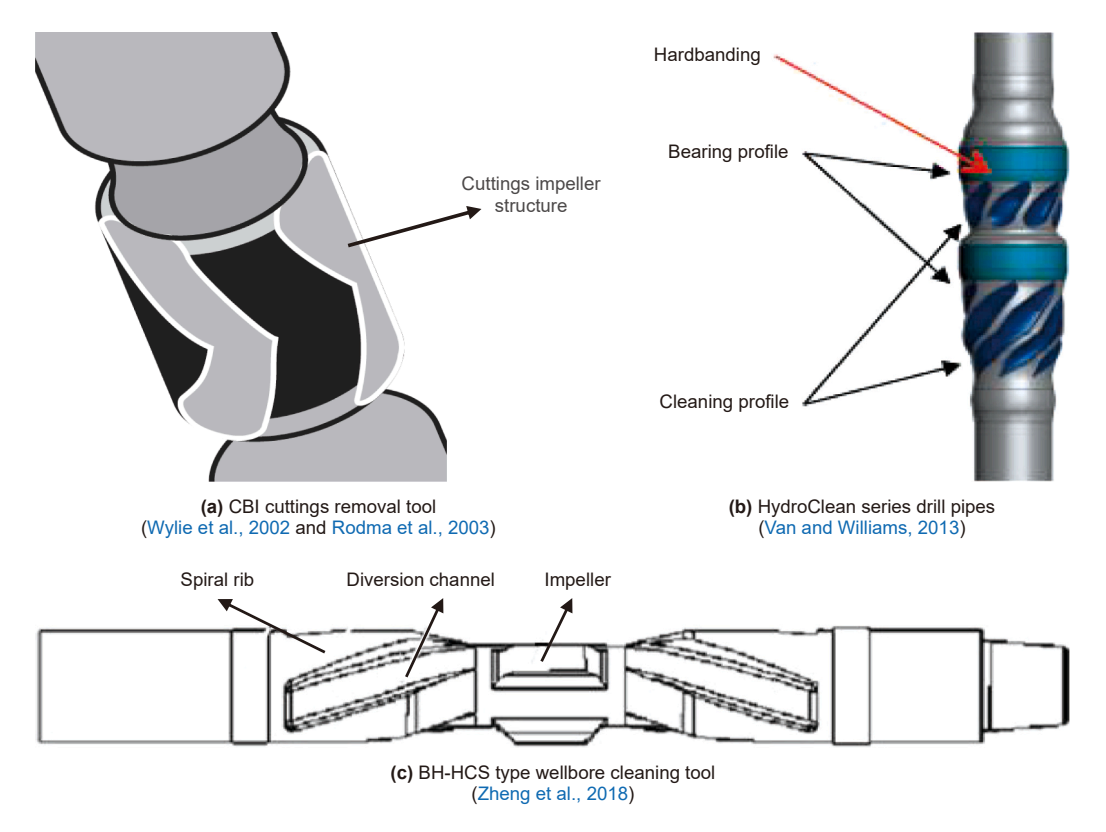


Fig. 1. Non-self-rotating cuttings removal tools.

stage of settling, cuttings particles begin to sink under the influence of gravity. Due to the small initial settling velocity v, the viscous resistance  $F_{\rm D}$  is also small. Under this condition, the buoyant weight  $F_{\rm B}$  on the cuttings particles exceed the viscous resistance  $F_{\rm D}$ , resulting in an increasing settling velocity v of the particles. As the settling velocity v increases, the cuttings particles experience an increasing viscous resistance  $F_{\rm D}$  until it balances out with the buoyant force  $F_{\rm B}$ , i.e.,  $F_{\rm B} = F_{\rm D}$ . At this point, the cuttings particles settle at a constant velocity. This constant settling velocity is the final settling velocity  $v_{\rm t}$  of the cuttings particles. Hence, there exist:

$$\frac{\pi d_{\rm S}^3}{6}(\rho_{\rm S}-\rho_{\rm l}){\rm g} = C_{\rm D}\frac{\pi d_{\rm S}^2}{4}\frac{\rho_{\rm l}\nu_{\rm t}^2}{2} \eqno(4)$$

According to Eq. (4), the final settling velocity of cuttings particles is expressed as:

$$v_{t} = \sqrt{\frac{4}{3} \frac{1}{C_{D}} \frac{\rho_{S} - \rho_{l}}{\rho_{l}} g d_{s}}$$
 (5)

In Eq. (5), only  $C_D$  is the unknown variable. Therefore, the resistance coefficient  $C_D$  must be determined to slove the final settling velocity  $v_t$  of cuttings particles. The resistance coefficient  $C_D$  is related to the particle Reynolds number  $Re_p$ . The physical significance of the particle Reynolds number is the ratio of the inertial force to the viscous force experienced by the particles during their motion. The expression for the particle Reynolds number  $Re_p$  is given by:

$$Re_{\rm p} = \frac{\rho_1 \nu_{\rm t} d_{\rm s}}{\mu_{\rm l}} \tag{6}$$

In Eq. (6):  $v_t$  represents the final settling velocity of cuttings particles, m/s, and  $\mu_l$  represents the viscosity of the drilling fluid, Pa·s.

Based on extensive drilling site data, Moore proposed a method to calculate the final settling velocity of cuttings particles. This method divides the fluid into three states based on the particle Reynolds number  $Re_p$ : laminar state ( $Re_p < 1$ ), transitional state ( $1 \le Re_p \le 2000$ ) between laminar and turbulent flow, and turbulent state ( $Re_p > 2000$ ). Consequently, the resistance coefficient corresponds to three different expressions:

The resistance coefficient curve is a straight line when the particles Reynolds number  $Re_p < 1$ . It can be assumed that the drilling fluid around the cuttings particles is in a laminar state. The expression for the final settling velocity of cuttings particles is:

$$v_{\rm t} = 0.33 \frac{d_{\rm s}^2(\rho_{\rm s} - \rho_{\rm l})g}{\mu_{\rm l}} \tag{7}$$

When  $1 \le Re_p \le 2000$ , the drilling fluid around the cuttings particles is transitional. The expression for the final settling velocity of cuttings particles is:

$$v_{t} = 0.153 \frac{d_{s}[g(\rho_{s} - \rho_{l})]^{0.667}}{\rho_{l}^{0.333} \mu_{l}^{0.333}}$$
 (8)

When  $Re_p > 2000$ , the resistance coefficient  $C_D$  remains essentially unchanged with the variation of the particle Reynolds number. At this point, the resistance coefficient is approximately equal to 1.5, that is,  $C_D = 1.5$ . The drilling fluid around the cuttings particles is in a turbulent state. The expression for the final settling velocity of cuttings particles is:

$$v_{\rm t} = 0.942 \sqrt{\frac{g(\rho_{\rm s} - \rho_{\rm l})d_{\rm s}}{\rho_{\rm l}}} \tag{9}$$

The final settling velocity of cuttings particles proposed by Moore is calculated in vertical wells, neglecting the impact of

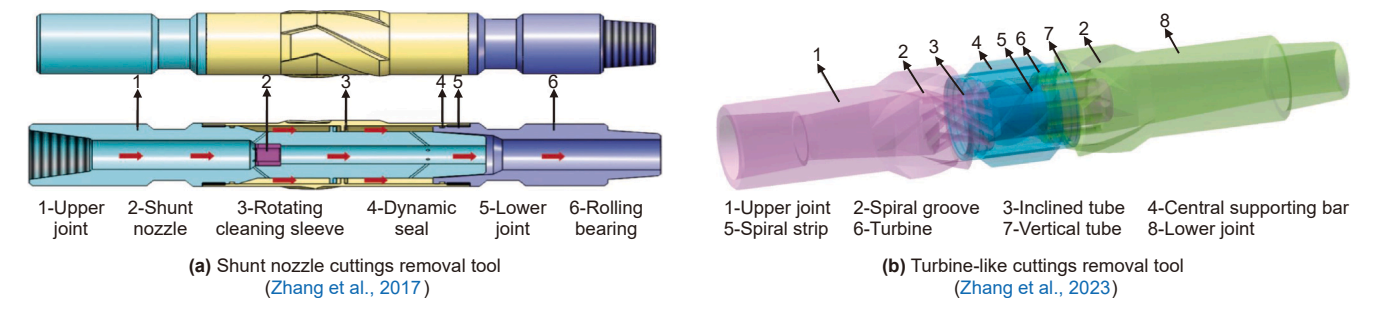


Fig. 2. Self-rotating cuttings removal tools.

cuttings collision. In the drilling process of highly deviated and horizontal wells, cuttings experience collisions between cuttings, cuttings and the wellbore wall, and cuttings and the drilling tools, as shown in Fig. 4. Therefore, the actual settling velocity of cuttings particles under practical conditions is smaller than the settling velocity proposed by Moore, requiring a modification to Moore's expression. Using the correction coefficient  $\Delta = 10$  proposed by Liu et al. (2016) based on experiments for correction, the corrected final settling velocity of cuttings particles, denoted as  $v_{ts}$ , is expressed as:

$$v_{\mathsf{ts}} = \frac{v_{\mathsf{t}}}{\Delta} = \frac{v_{\mathsf{t}}}{10} \tag{10}$$

After simplification by correction coefficients, the movement of cuttings particles in actual wellbores can be viewed as a parabolic motion, as shown in Fig. 5. In the direction of the wellbore axis, they experience the effect of upward returning drilling fluid, with their velocity equal to the annular return velocity of the drilling fluid. Along the direction of gravity, they undergo free settling motion. The following assumptions are made: cuttings particles start settling from the high side of the wellbore and cease movement upon reaching the low side, forming a stationary cuttings bed; the cuttings are smooth, uniformly shaped, and circular particles. Considering the influence of the wellbore inclination, the displacement of cuttings particles can be determined, expressed as follows:

$$l = \frac{D_1 \, \nu_{\rm h}}{\sin(\theta) \, \nu_{\rm ts}} \tag{11}$$

In Eq. (11):  $v_{\rm h}$  represents the annular return velocity of the drilling fluid, m/s;  $\theta$  denotes the wellbore inclination angle, °; l stands for the displacement of cuttings particles, m;  $D_1$  represents the diameter of the wellbore, mm.

### 2.2. Installation position of VCRT

Taking the highly deviated well Z401X in an eastern oilfield in China as an example, based on the corrected model for annular cuttings settling and removal in the wellbore, the sections prone to forming cuttings beds in this well can be calculated. This enables the determination of the installation location for the VCRT.

The three-dimensional well trajectory of the Z401X well follows a seven-stage system: vertical-increasing-stable-increasing-stable-decreasing-stable. The 0–500 m section is a vertical interval with 0° inclination; the 500–1080 m interval is a build-up section where the inclination increases from 0° to 34.80°; the 1080–1128 m interval is a tangent section with the inclination maintained at 34.80°; the 1128–1399 m interval is a build-up section where the inclination increases from 34.80° to 38.97°; the 1399–2180 m interval is a tangent section with the inclination held at 38.97°; the 2180–2447 m interval is a drop section where the inclination decreases from 38.97° to 24.21°; and the 2447–2635 m interval is a tangent section with the inclination maintained at 24.21°. The well trajectory design is presented in Table 1.

The data presented in this table demonstrates that, in instances where the well depth exceeds 800 m, the average inclination angle is approximately 30°. The cuttings generated by drilling with PDC bits, which have higher wear levels, are fine when drilling conditions are above, characterized explicitly by high rotational speed, low weight on bit, and high flow rate. The particle diameters of these cuttings range from a maximum of 2–3 mm, typically between 0.5 and 1 mm, or even in a powdered form. In light of the evidence mentioned above, this paper makes the following assumptions based on a practical examination of the Z401X: the inclination angle of well Z401X is 30°, and the cuttings are smooth,

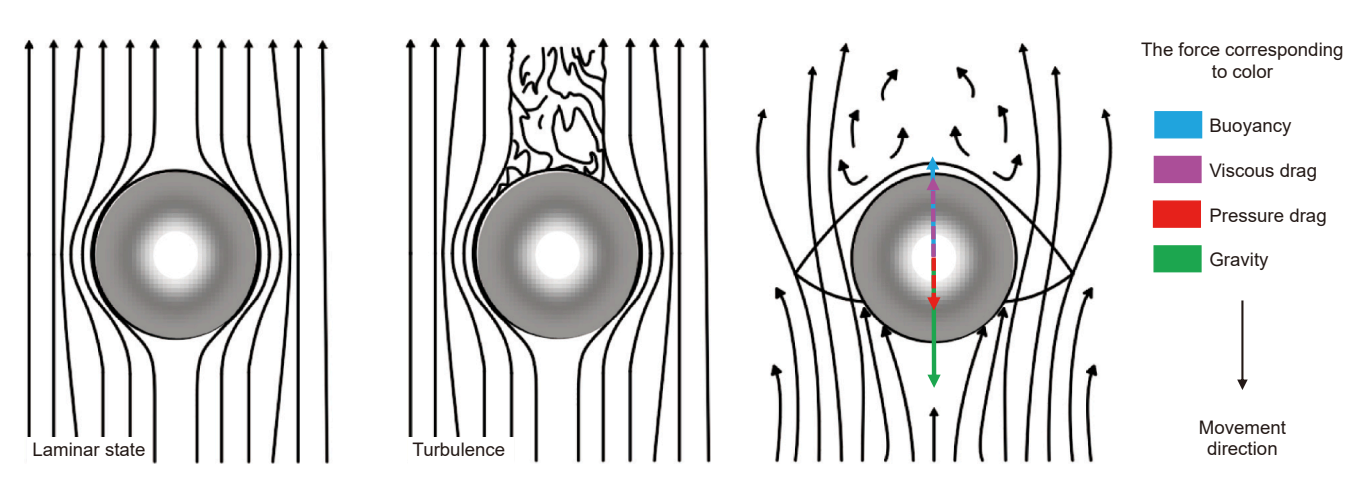


Fig. 3. Analysis of force characteristics of cuttings particles during settling motion.

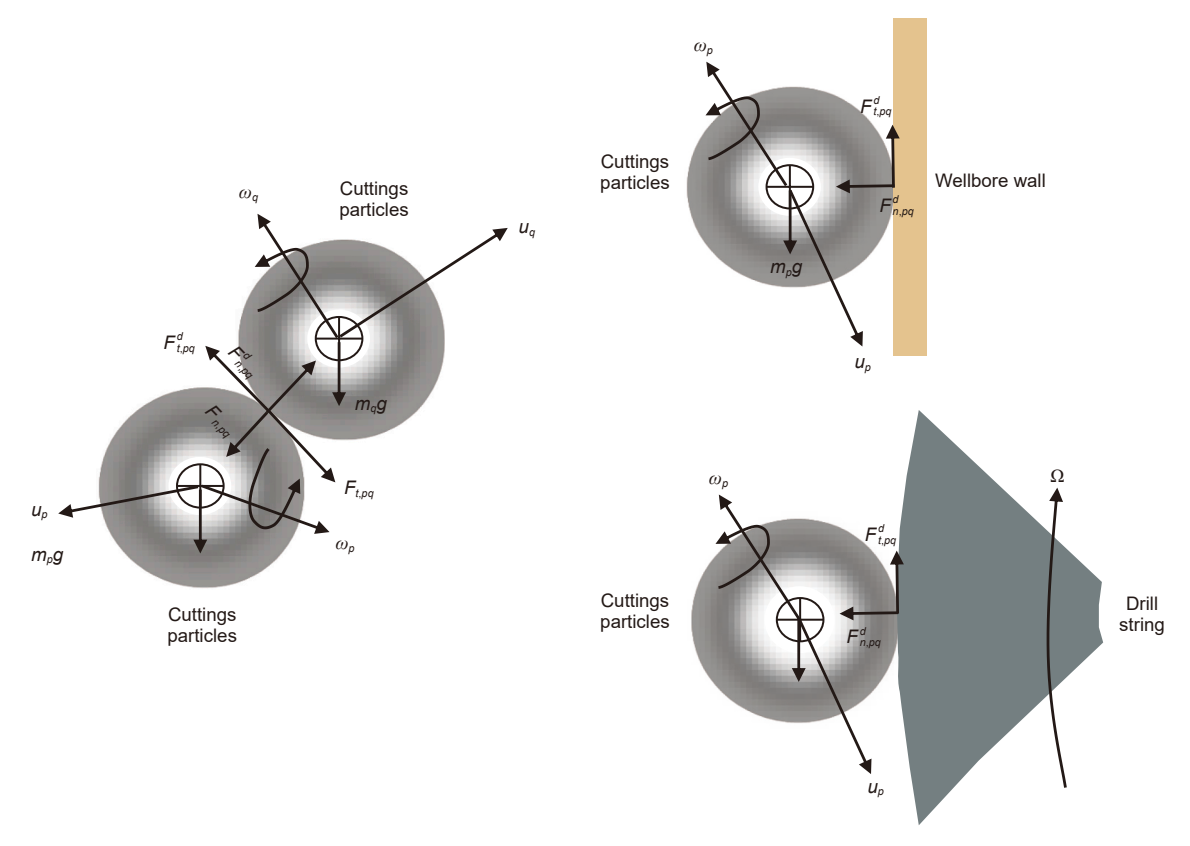


Fig. 4. The force distribution of cuttings particles in the wellbore.

uniform, and circular particles with a diameter of 1.5 mm. The relevant characteristic parameters of well Z401X are presented in Table 2.

Assuming the particle Reynolds number between 1 and 2000, the expression for the settling terminal velocity of cuttings is:

$$\nu_{\rm t} = 0.153 \frac{d_{\rm s}[g(\rho_{\rm s} - \rho_{\rm l})]^{0.667}}{\rho_{\rm l}^{0.333} \mu_{\rm l}^{0.333}} \tag{12}$$

By substituting the data from Table 2 into Eq. (12), the value of  $v_t$  was calculated to be 0.0289 m/s. After substituting  $v_t$  into Eq. (6), the particle Reynolds number  $Re_p$  is calculated to be 1.15 ( $Re_p = 1.15$ ), indicating that the selected particle Reynolds number is reasonable.

Substitution of the value of  $V_{\rm ts}$  into Eq. (10) allows the corrected terminal settling velocity of cuttings particles,  $v_{\rm ts}$ , to be calculated as 0.00289 m/s ( $v_{\rm ts}=0.00289$  m/s). Substitution of  $v_{\rm ts}$  into Eq. (11) yields that the removal distance of cuttings, l, equals 187.53 m (l=187.53 m). In the text, after the bit breaks the rock, a cuttings bed tends to form in the well section approximately 188 m away from the bit. Therefore, the VCRT can be installed at a position about 188 m from the bit.

In practical engineering, factors such as wellbore inclination angle, ROP, and formation characteristics significantly influence the installation position of cuttings removal tools. The actual installation position of the VCRT tool should be determined based on field-specific parameters combined with the model proposed in this study.

### 3. Analysis of VCRT simulation application effectiveness

According to the modified annular cuttings settling and removal model, it is calculated that the VCRT should be installed in the Z401X well at a position approximately 188 m away from the

bit. Based on this, a CFD model of the annular flow field is established, and numerical simulation methods are employed to analyze the effectiveness of VCRT in clearing cuttings in the well.

### 3.1. Structure design and working principle of VCRT

The VCRT comprises the upper joint, lower joint, spiral channel, rotor sleeve, rotating blade, stator and rotor assembly, as illustrated in Fig. 6.

The VCRT has a turbine-like structure, which differs from traditional designs. In a traditional turbine, the rotor is located inside the stator, and the rotor drives the inner core shaft to rotate. In contrast, the turbine-like structure features an externally positioned rotor relative to the stator, with the rotor driving rotating blades affixed to it. This turbine-like structure is shown in Fig. 7(a). The turbine-like structure described in this paper consists of multiple turbine-like stages, each containing one stator and one rotor (as shown in Fig. 7). The model in this study comprises eight such turbine-like stages.

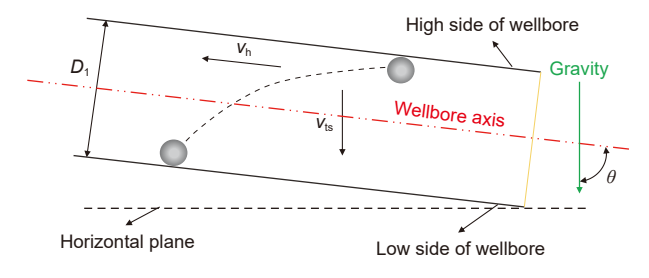


Fig. 5. Simplified model for the removal of cuttings particles in wellbore.

F. Chen, H.-L. Lu, Z.-H. Liu et al. Petroleum Science 22 (2025) 3787–3802

**Table 1**Table of Z401X deviated wellbore trajectory design.

Well depth, m	Well inclination, °	Vertical depth, m	Well depth, m	Well inclination, °	Vertical depth, m
0	0.00	0.00	1399	38.97	1305.00
500	0.00	500.00	2180	38.97	1924.98
600	6.00	599.82	2217	35.57	1955.00
800	18.00	795.09	2350	29.01	2067.08
950	27.00	933.53	2447	24.21	2153.97
1080	34.80	1045.03	2536	24.21	2235.00
1128	34.80	1084.62	2635	24.21	2325.00
1250	35.20	1184.47	1	1	1

**Table 2**Relevant characteristic parameters of well.

Parameter categories	Parameter sizes
Diameter of cuttings particle $d_s$ , mm	1.5
Drilling fluid dynamic viscosity $\mu_1$ , Pa·s	0.045
Wellbore diameter D <sub>1</sub> , mm	215.9
Annular return velocity of drilling fluid $v_h$ , m/s	1.25
Density of cuttings particles $\rho_s$ , kg/m <sup>3</sup>	2250
Density of drilling fluid $\rho_1$ , kg/m <sup>3</sup>	1200
Wellbore inclination angle $\theta$ , $^{\circ}$	30

The drilling fluid first flows through the upper joint into the turbine-like area; the flow process is shown in Fig. 7(b). The spiral channel serves as a righting mechanism. When the drilling fluid impacts the turbine-like structure, it causes the rotor to rotate, thereby driving its affixed rotating blade synchronously. During sliding drilling, this blade rotation throws cuttings deposited on the annulus's lower side to the upper side, achieving effective cuttings removal.

## 3.2. Determination of two-phase flow model and analysis of annular flow field characteristics

The flow in the annular space, under the application of cuttings removal tools, involves a two-phase flow of drilling fluid (liquid phase) and cuttings particles (solid phase). The mixture model is chosen as the two-phase flow calculation model in this study,

while the realizable-*k*- $\varepsilon$  model is selected as the turbulence calculation model. Boundary layer theory and wall functions are analyzed, and the Standard Wall Function (SWF) is chosen to ensure adequate data acquisition near the wall. The characteristics of flow velocity distribution, pressure distribution, streamline variations, and cuttings removal under the influence of VCRT and conventional drilling tools are analyzed. The results indicate a significant improvement in cuttings removal efficiency after installing VCRT.

### 3.3. VCRT flow field CFD model

Only the PDC bit, Drill Collar (DC), VCRT, and Heavy-Weight Drill Pipe (HWDP) in the drill string combination are retained to simplify the calculation. The physical model of the VCRT flow field in well Z401X is shown in Fig. 8. The model is comprised of five distinct parts. The first part is the bit fluid domain, which has a length of  $L_1$ ; the second part is the DC fluid domain, which has a length of 44,000 mm; the third part is the HWDP fluid domain, which has a length of 44,000 mm; the third part is the HWDP fluid domain, which has a length of 44,000 mm. The fourth component is the VCRT fluid domain, which has a length of 44,000 mm. The fourth component is the HWDP fluid domain, which has a length of 44,000 mm. The fifth component is the HWDP totaling 40,000 mm. The bit is a standard PDC bit with a DC outer diameter of 40,000 mm. The bit is a standard PDC bit with a DC outer diameter of 40,000 mm. The lit is a standard PDC bit with a DC outer diameter of 40,000 mm. The lit is a standard PDC bit with a DC outer diameter of 40,000 mm. The lit is a standard PDC bit with a DC outer diameter of 40,000 mm. The lit is a standard PDC bit with a DC outer diameter of 40,000 mm. The lit is a standard PDC bit with a DC outer diameter is 40,000 mm, and the inner diameter is

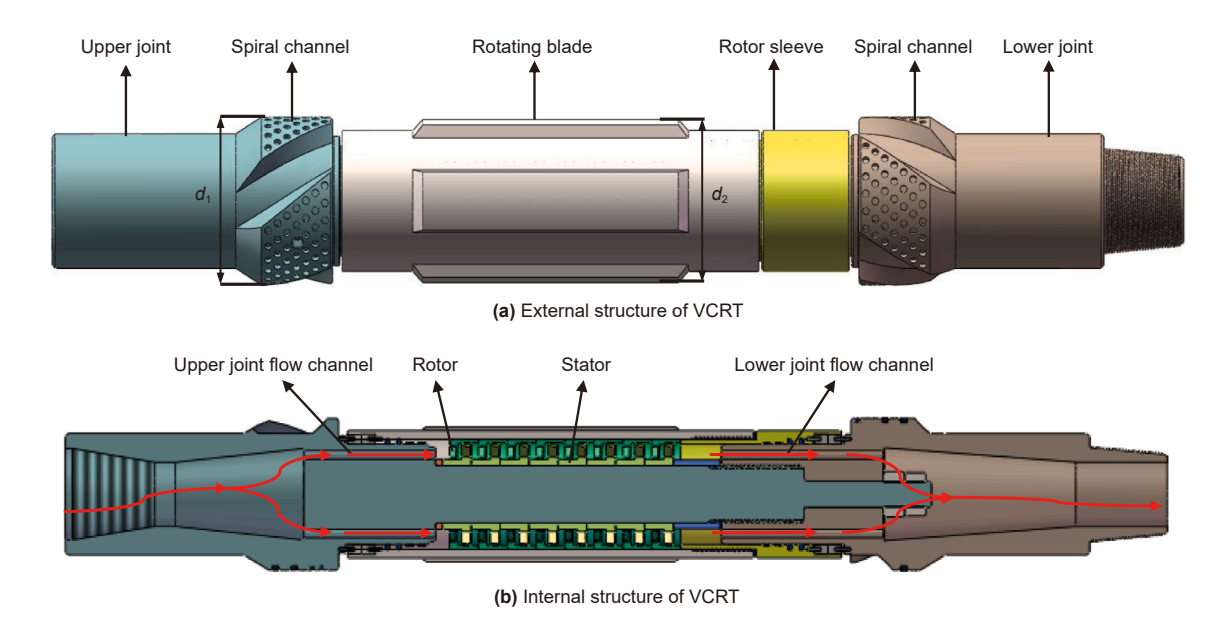
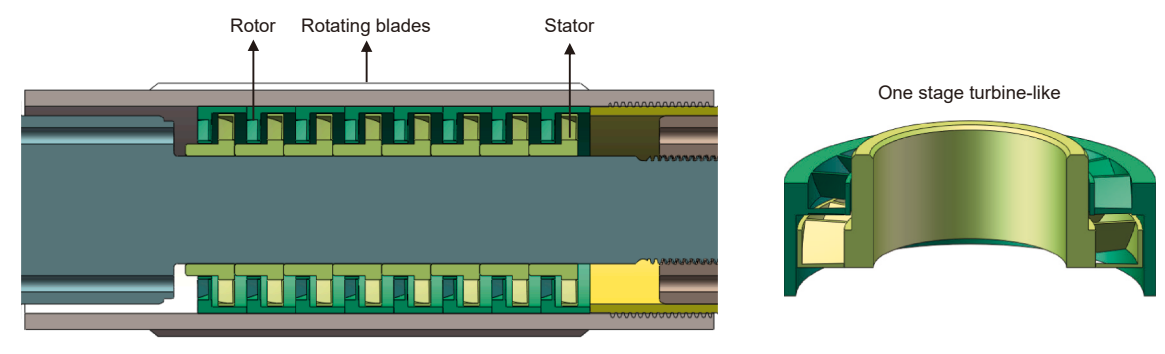


Fig. 6. The structure of VCRT.



(a) The assembly structure of turbine-like and rotating blade

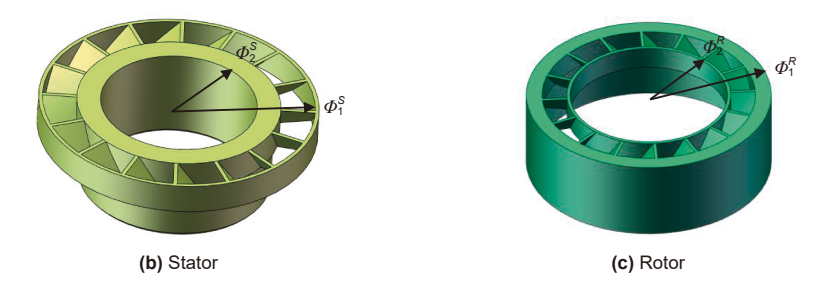


Fig. 7. The structure of turbine-like.

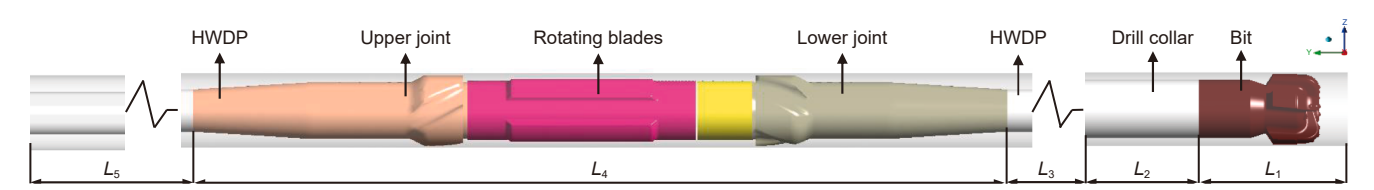


Fig. 8. Physical model of VCRT flow field in well Z401.

76.2 mm. The dimensions of the physical model are presented in Table 3.

The inlet velocity of the drilling fluid is 6.5 m/s (displacement 30 L/s, with the inner diameter of the weighted drill collar being 76.2 mm), and the outlet is a pressure outlet (30 MPa, same as the external pressure). The drilling fluid density is  $1200 \, \text{kg/m}^3$ , and the drilling fluid viscosity is  $0.045 \, \text{Pa-s}$ . The density of cuttings particles is  $2250 \, \text{kg/m}^3$ , assuming the particle diameter to be  $1.5 \, \text{mm}$  and the well deviation angle to be  $30^\circ$ . The rotating blades rotate only about the axis; therefore, only the rotational degrees of freedom about the axis are enabled, while other degrees are constrained. The rotating domain of the blades is set as a rigid body

**Table 3** Physical model dimension parameters.

Parameter categories	Parameter sizes, mm		
Length of bit fluid domain $L_1$	400.0		
Length of drill collar fluid domain $L_2$	44,000.0		
Length of HWDP fluid domain $L_3$	144,000.0		
Length of VCRT fluid domain $L_4$	1600.0		
Length of HWDP fluid domain $L_5$	18,000.0		
Wellbore diameter D <sub>1</sub>	215.9		
Spiral channel diameter $d_1$	214.0		
Rotating blades outer diameter $d_2$	206.0		
Drill collar outer diameter	165.1		
Drill collar inner diameter	71.4		
Outer diameter of HWDP	127		
Inner diameter of HWDP	76.2		

**Table 4** Mesh independence analysis.

Number of mesh	Pressure of drop, Pa/m	Relative error, %	
2,851,738	76,821		
3,323,182	83,899	9.20	
3,653,621	87,125	3.80	
4,115,654	87,479	0.41	

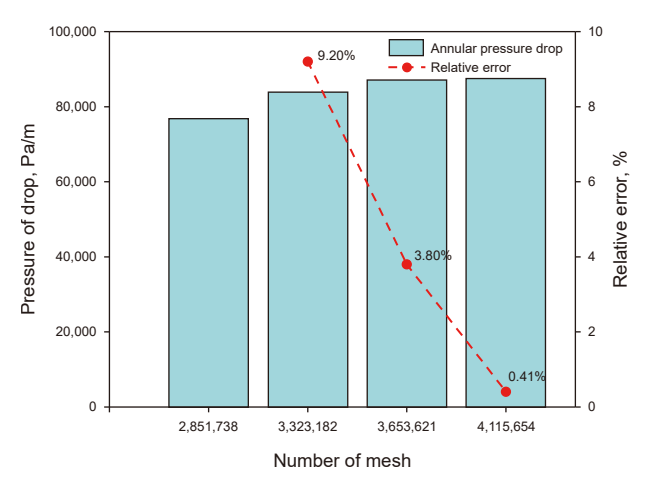


Fig. 9. Mesh independence analysis.

passive motion domain, with the blades and rotor wall defined as passive motion walls and all other walls as fixed walls.

Mesh size significantly impacts the simulation results; thus, a mesh independence analysis was conducted. Four different numbers of meshes are used for the mesh independence analysis (2,851,738 meshes, 3,323,182 meshes, 3,653,621 meshes, and 4,115,654 meshes), as shown in Table 4. Fig. 9 illustrates the variation in annular pressure drop for models with different numbers

of meshes. The results indicate that when the mesh count reaches 4115654, the annular pressure drop changes very little compared to when the number of meshes is 3,653,621, with only a 0.41% difference. Therefore, 3,653,621 meshes are selected for the model.

The fluid domain where the bit and VCRT are located adopts 6 mm meshes, while the surface of the bit and VCRT adopts 3 mm meshes. Other fluid domains adopt 10 mm meshes. The mesh model is depicted in Fig. 10.

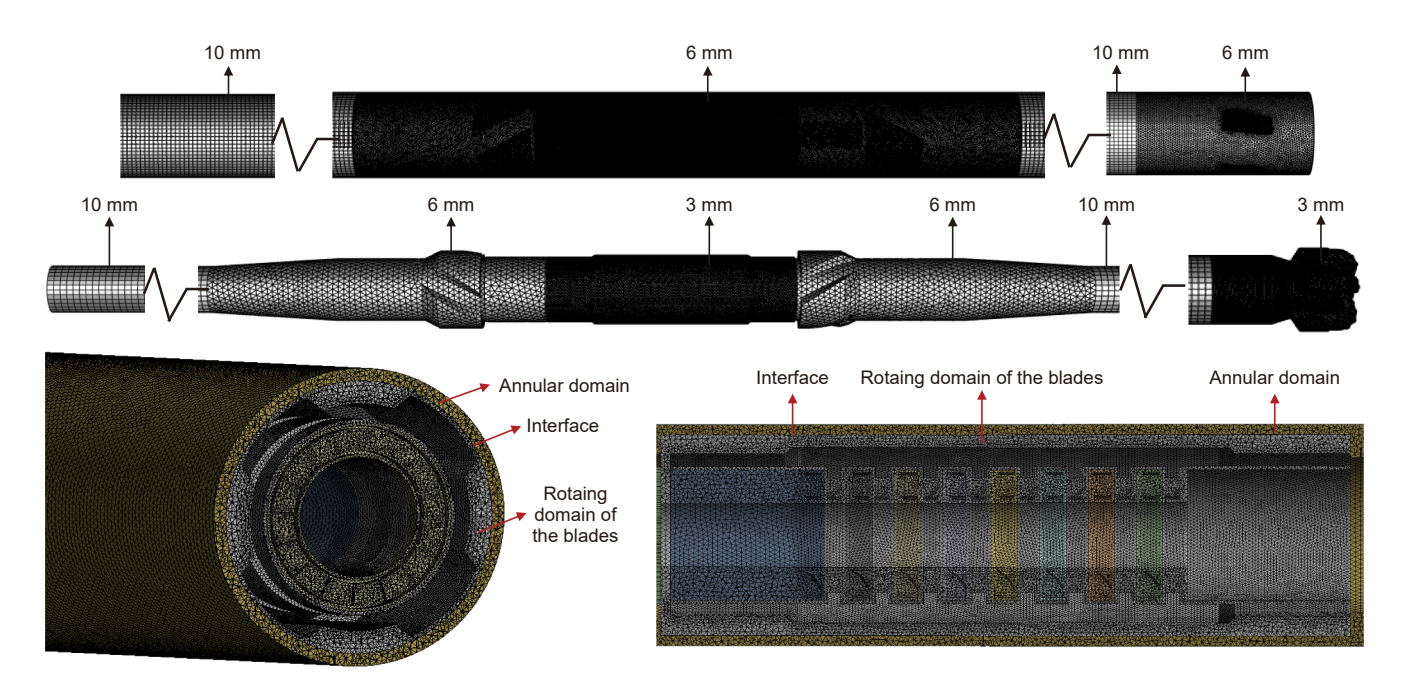
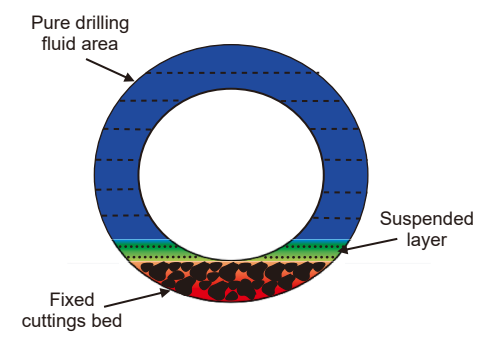
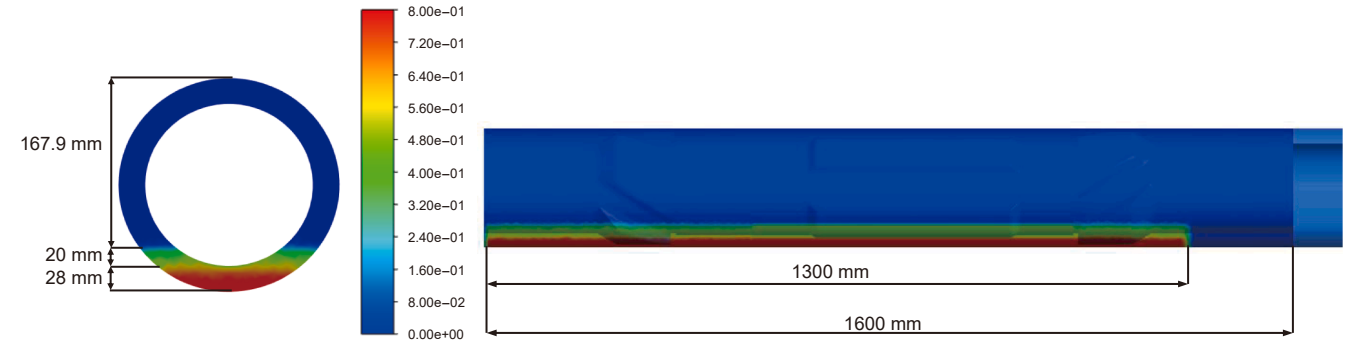


Fig. 10. Mesh model of VCRT in well Z401X



(a) Three-layer model geometry



(b) Initial cuttings distribution diagram

Fig. 11. Cuttings model in initial state.

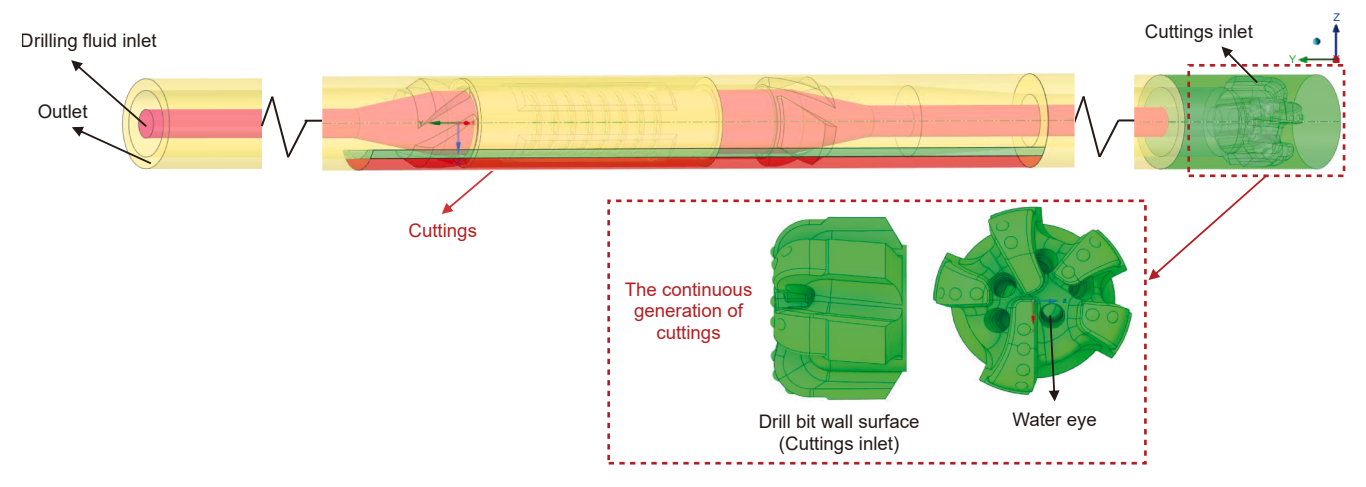


Fig. 12. Cuttings model for the entire well section.

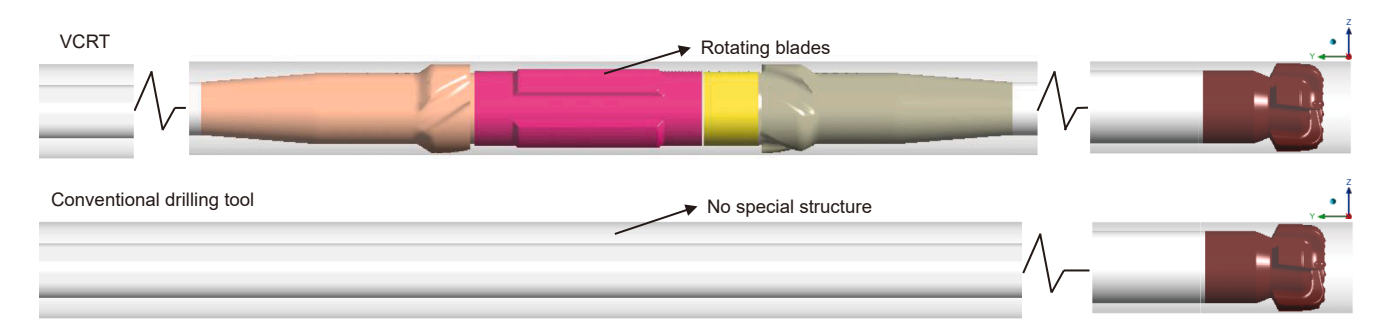


Fig. 13. VCRT and conventional drilling tool models.

There are four different fluid dynamic models for cuttings transport: uniform suspension, non-uniform suspension, moving bed, and fixed bed flow. Based on previous experimental studies, the computational accuracy of the three-layer cuttings transport model is higher than that of the two-layer model. Therefore, the three-layer model is used in this paper (Han, 2023). The model assumes the following: 1) The bottom layer is a fixed cuttings bed with a height of 28 mm and a cuttings volume fraction of 0.8. This layer is uniformly filled with constant bed porosity; 2) The middle layer consists of a mobile suspension layer with a height of 20 mm and a cuttings volume fraction of 0.5 (Zhang et al., 2024); 3) The upper layer of the cuttings bed is distributed in the fluid domain of the VCRT, with a bed length of 1300 mm. The initial distribution of the cuttings bed is shown in Fig. 11.

During the drilling process, cuttings are generated by the bit, which breaks the rock and continuously mixes them into the drilling fluid. Therefore, the bit is designated as the cuttings inlet with a cuttings volume fraction set to 0.54% (In well Z401X, the ROP is approximately 16 m/h, the wellbore diameter is 215.9 mm, the volume of rock broken by the bit is around 0.16 L/s, and the drilling fluid flow rate is 30 L/s, which results in the proportion of cuttings produced per second by the bit to the volume of the drilling fluid with cuttings being around 0.53%). The bit rotates at 180 rpm, and the cuttings model for the entire well section is shown in Fig. 12.

### 3.4. Analysis efficiency of cuttings removal VCRT

Fig. 13 displays a comparative analysis of VCRT's effectiveness in removing cuttings in well Z401X, comparing it to traditional drilling tools.

Cross-section A and path 1, located on the lower side of the wellbore within the fluid domain, were selected to facilitate the evaluation of cuttings efficiency under VCRT and conventional drilling tools. Cross-section A is positioned within the HWDP segment, while path 1 extends from the VCRT inlet to the outlet. The locations of both cross-section A and path 1 are shown in Fig.

Considering the rotational inertia of both the turbine-like rotor and the rotating blades and neglecting internal friction in the VCRT, the rotational velocity of the VCRT blades propelled by drilling fluid is determined through simulation analysis, as shown in Fig. 15. The results indicate that the blades initially remain stationary. The impact of drilling fluid drives the turbine-like structure to push against the rotor and attached blades. The blade rotational speed gradually increases until reaching a steady state. At approximately 0.6 s, the rotational speed achieves 430 rpm and stabilizes at this value.

Fig. 16 displays the overall pressure fluctuation in the flow field influenced by VCRT. The data indicate that the total pressure at the first-stage turbine-like segment initially measures 32.2 MPa, decreasing to 30.7 MPa after passing through eighth-stage turbine-like section. From the first turbine-like stage onward, a continuous pressure decline occurs with a total drop of 1.5 MPa when the drilling fluid flows through the turbine-like region.

Fig. 17(a1)–(e1) illustrates the cuttings distribution patterns under VCRT and conventional drilling tools over 0–20 s. The results demonstrate that at t=0 s, the cuttings bed remains in its initial configuration, with the cuttings bed positioned at the wellbore bottom under both tools. At 5 s, both tools modify the cuttings bed: VCRT induces uniform annular cuttings distribution, whereas the conventional tools cause accumulation along the wellbore's lower edge. By 10 s, the VCRT-processed cuttings maintain uniform

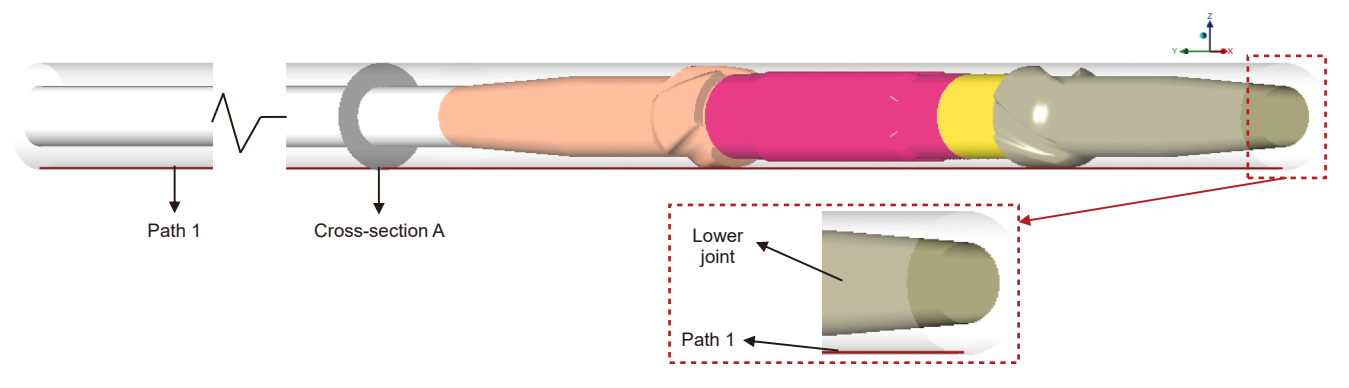


Fig. 14. Positions of cross-section A and path 1.

dispersion throughout the annulus, contrasting with the limited modification of conventional tools. At 15 s, the VCRT significantly reduces lower side cuttings while increasing annular concentration, whereas conventional drilling tools achieve only marginal

reduction. At 20 s, the drilling fluid transports cuttings toward the outlet, with VCRT-exposed zones showing lower cuttings than conventional tools. Fig. 17(a) further demonstrates the VCRT-driven cuttings bed disruption, where lower-edge cuttings are

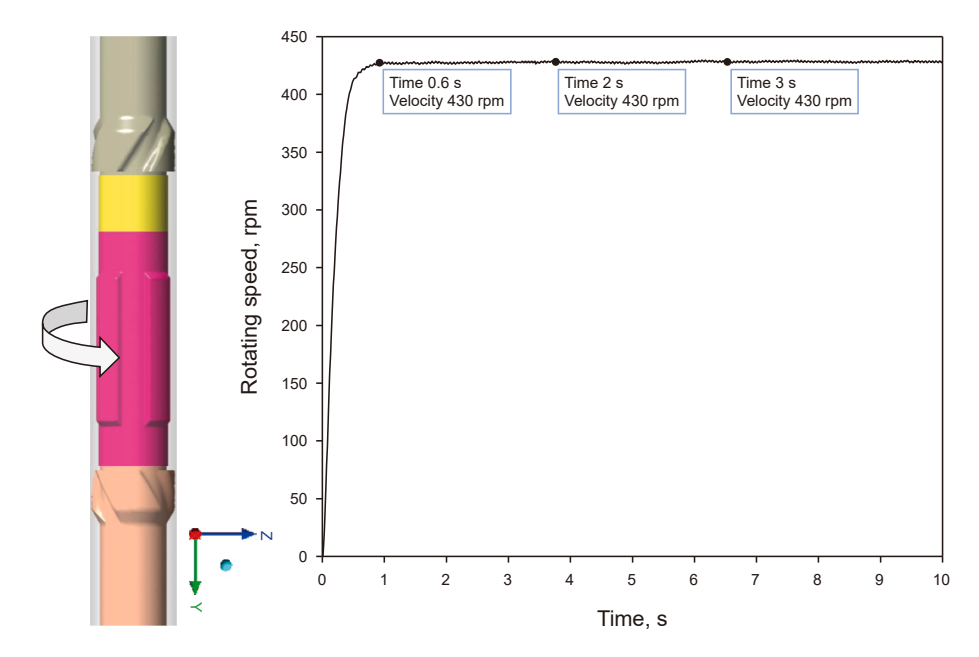


Fig. 15. VCRT rotating blade speed.

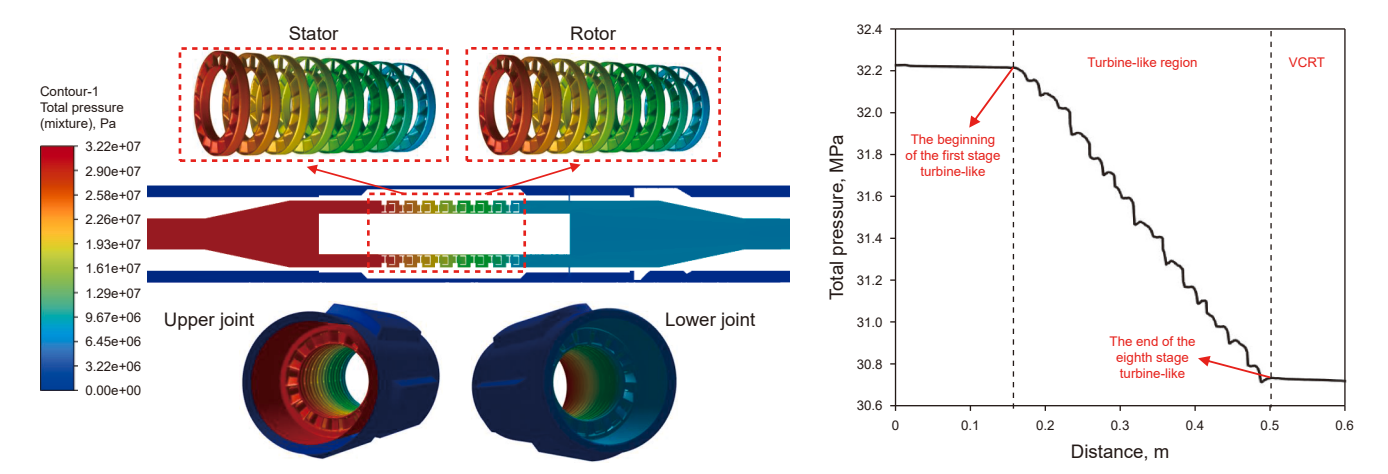


Fig. 16. Total pressure variation of flow field under the action of VCRT.

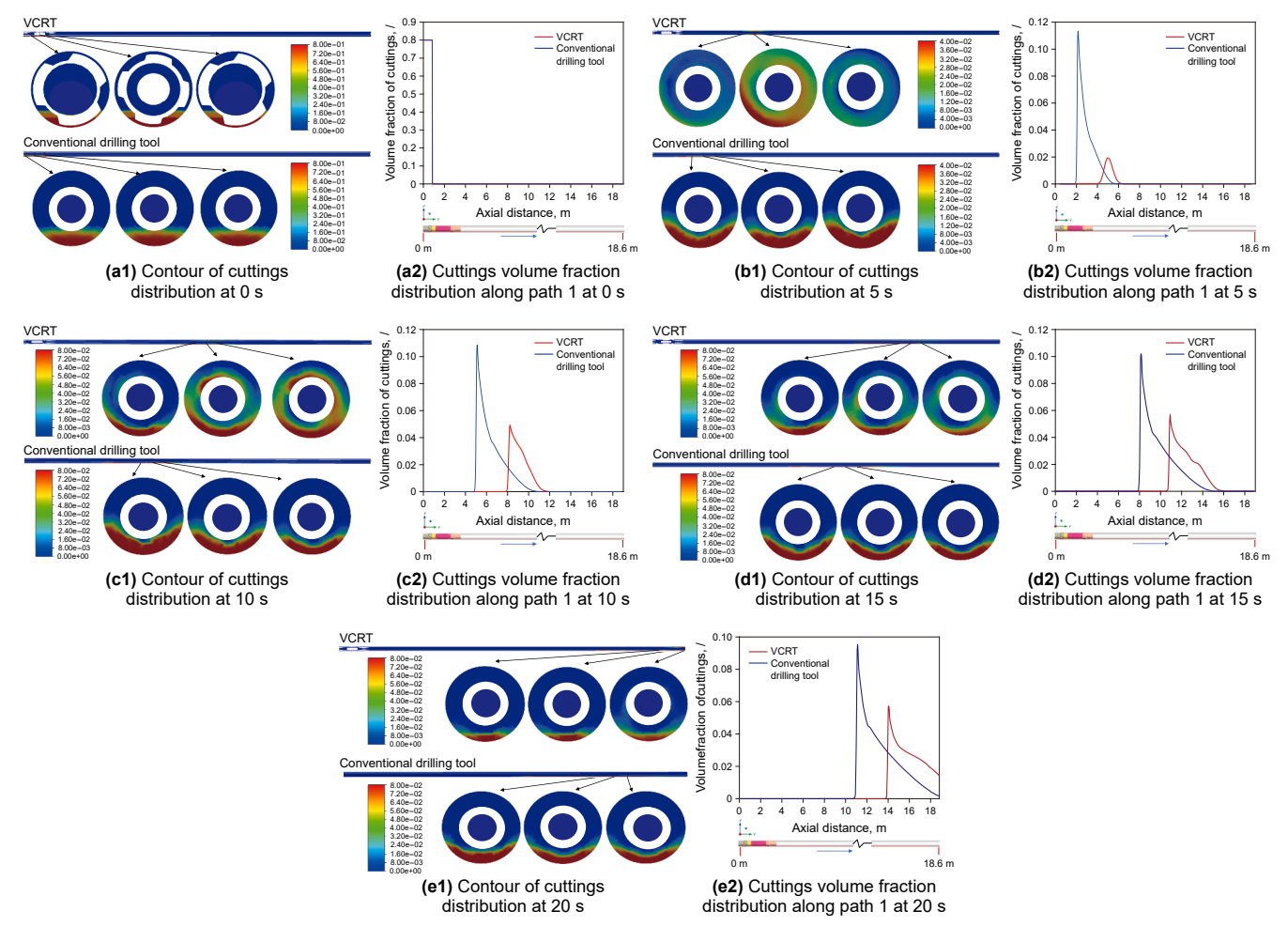


Fig. 17. Distribution of cuttings in the wellbore under the action of VCRT and conventional drilling tool within 0-20 s.

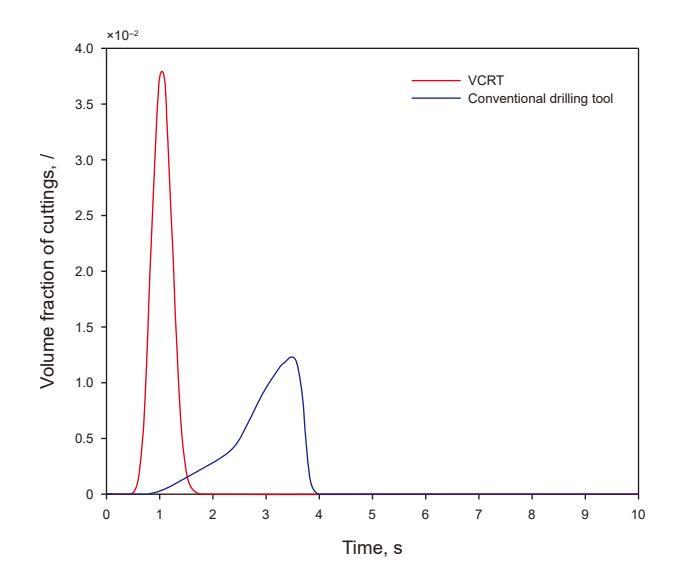
propelled upward and evacuated through the outlet. Conversely, conventional tools barely change the bed's morphology, preserving lower-edge accumulation.

Fig. 17(a2)–(e2) compares cuttings volume fraction profiles along path 1 under both tools during 0–20 s. Initially, both systems have identical distributions. By 5 s, VCRT achieves outlet-proximal evacuation with a 60% lower volume fraction than conventional tools. This disparity persists at 10, 15, and 20 s. After 20 s, the analysis reveals a conventional tool mean fraction of 0.011 versus 0.007 (36.43% reduction) with VCRT, confirming its superior performance.

Fig. 18 illustrates the cuttings volume fraction variation at cross-section A under VCRT and conventional drilling tools from 0 to 10 s. Observation indicates that with VCRT, the fraction starts rising at 0.5 s and declines sharply at 2 s, showing most cuttings have passed through. For conventional tools, the fraction begins to increase at 1 s. By 4 s, most cuttings have passed through. VCRT exhibits higher cuttings removal rates. Under VCRT, the mean fraction per unit time is roughly 0.016, compared to about 0.0054 with conventional drilling tools. Thus, the average cuttings volume fraction passing through cross-section A per unit time under VCRT is roughly three times that under conventional drilling tools.

Fig. 19(a) demonstrates that VCRT operation generates a spiral flow in the drilling fluid, continuously scouring the wellbore's lower edge to disrupt the cuttings bed and prolonging cuttings suspension in the annulus. This spiral significantly enhances the drilling fluid's capacity to transport cuttings. Under conventional drilling

tools, the drilling fluid flows primarily axially without generating spiral flow, resulting in limited removal of axis-parallel cuttings and ineffective bed elimination. Fig. 19(b) displays the evolution of



**Fig. 18.** The curve of cuttings volume fraction variation through cross-section A within 0–10 s under the action of VCRT and conventional drilling tool.

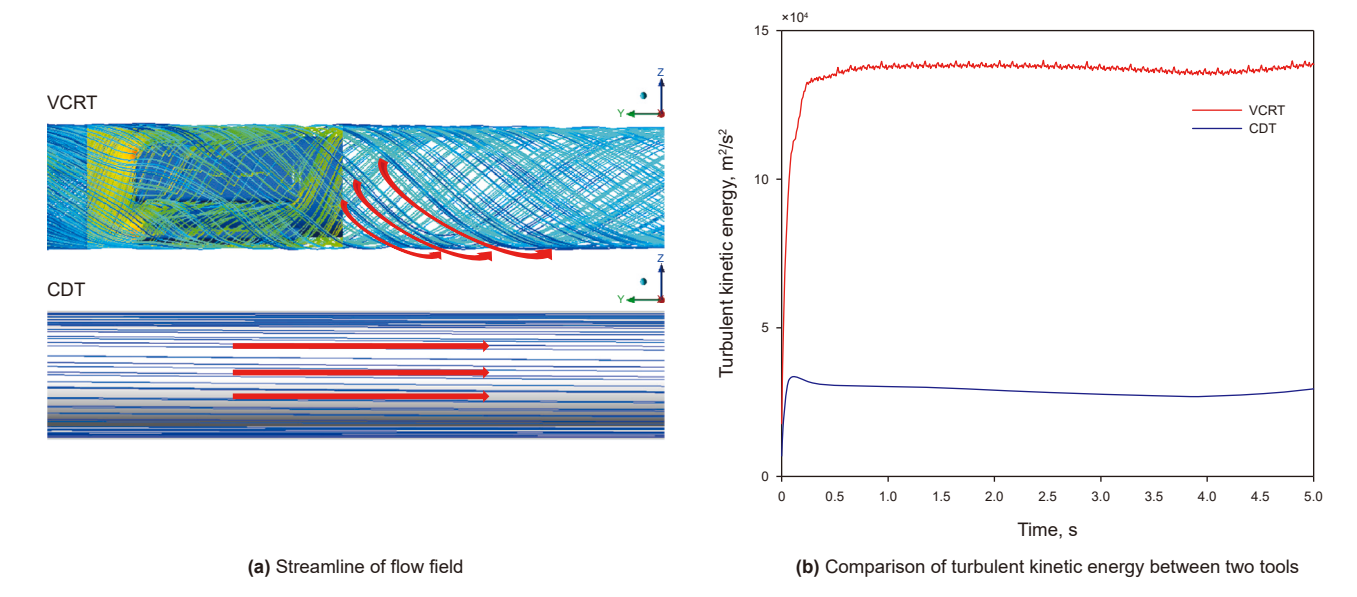


Fig. 19. Comparison of streamline and turbulent kinetic energy between two tools.

turbulent kinetic energy for both methods during the 0–5 s interval. The initial turbulent flow energy of the drilling fluid measures  $0 \, \text{m}^2/\text{s}^2$ . Over time, the turbulent kinetic energy increases progressively toward a state of stabilization. Under the action of VCRT, the turbulent flow energy remains stable at  $1.39 \times 10^5 \, \text{m}^2/\text{s}^2$ ,

while under the action of conventional drilling tools, it remains stable at  $2.94 \times 10^4 \, \text{m}^2/\text{s}^2$ . The turbulent kinetic energy under VCRT is about 4.7 times that under conventional drilling tools.

Analysis of the cuttings removal patterns under VCRT and conventional drilling tools shows that the volume fraction of

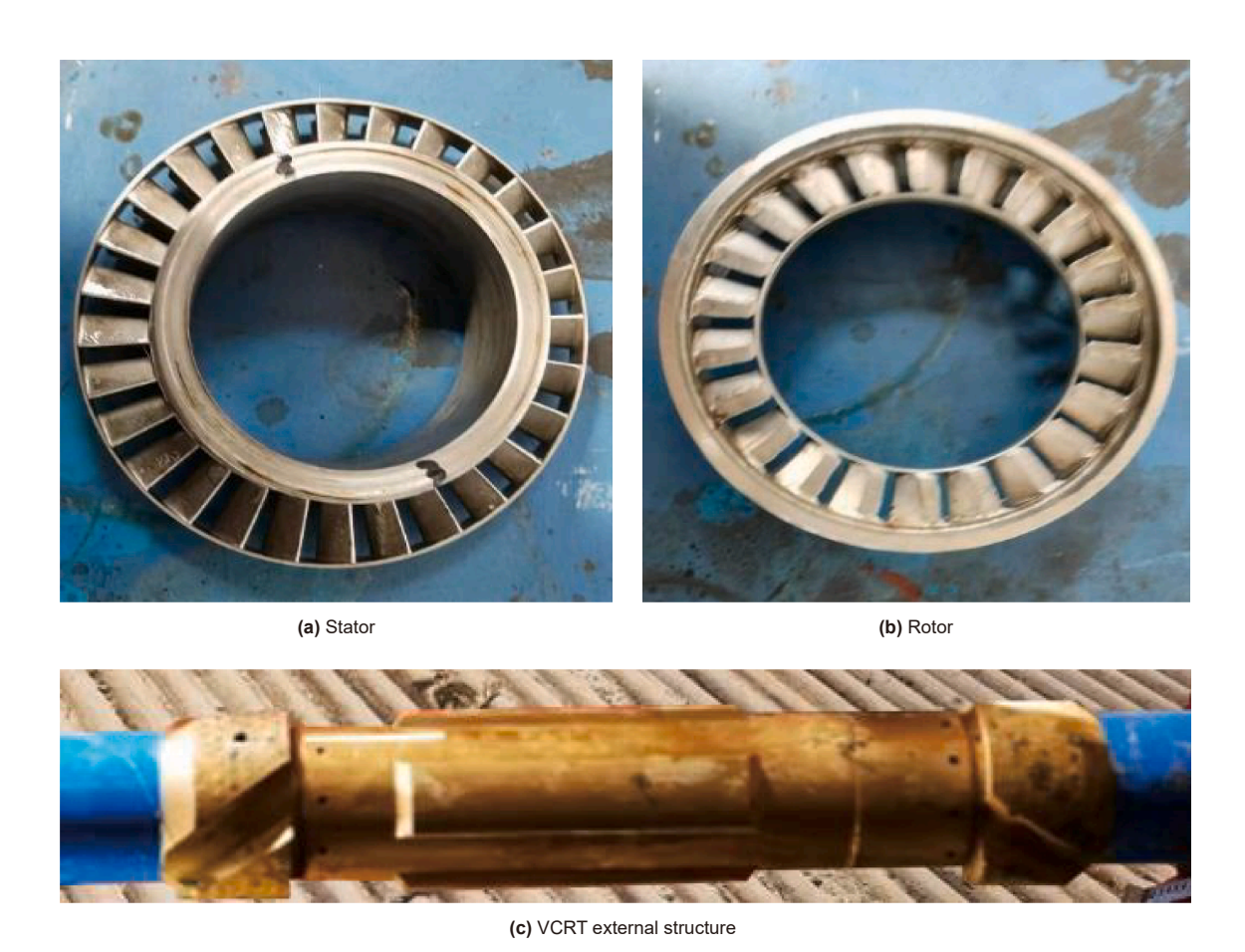


Fig. 20. VCRT physical schematic.

F. Chen, H.-L. Lu, Z.-H. Liu et al. Petroleum Science 22 (2025) 3787–3802

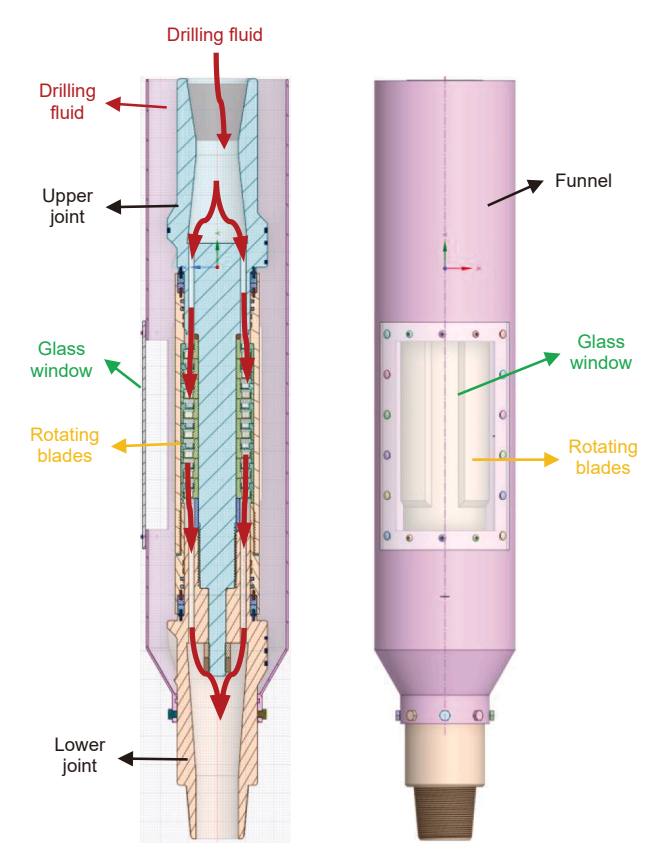


Fig. 21. Schematic diagram of experimental setup.

cuttings at the wellbore's lower side is significantly lower with VCRT. Furthermore, the removal velocity of cuttings is higher under VCRT. The high-speed rotation of VCRT impeller blades generates a spiral flow with greater turbulent kinetic energy, disrupting the cuttings bed and enabling rapid cuttings removal via the drilling fluid. Conventional tools, however, exert only axial scraping without significant disturbance, causing slow cuttings migration. Consequently, VCRT reduces lower-side cuttings and accelerates annular removal, improving overall efficiency.

20(b) depicts the rotor, and Fig. 20(c) illustrates the external structure of the VCRT.

The experiment was conducted in a metal funnel with an inner diameter greater than the exterior diameter of the VCRT, equipped with a glass observation window. The VCRT was placed inside the funnel, and drilling fluid was injected. Upon pump activation, the fluid flowed into the upper joint and activated the turbine blades through impact forces, driving the rotor to rotate. The blades in rotation rotated synchronously with the rotor. Rotation speed was measured through the window using a laser velocimeter. The experimental setup is shown in Fig. 21.

To ensure the accuracy of the numerical pressure drop results in the flow field, two controlled-variable experiments were performed. The initial experiment was described previously. For measuring pressure drop at the turbine-like structure, the second experiment removed this structure from the VCRT (with the rotating blades fixed stationary), allowing direct fluid flow from the upper to the lower joint.

The rotational behavior of the blades and the fluid field pressure drop under varying flow rates are summarized in Table 5. Data indicate that at 15 L/s drilling fluid flow rate, pressure drop reaches 0.7 MPa. Increasing the flow rate corresponds to a corresponding elevation in pressure drop, achieving 1.6 MPa at 30 L/s. Initial blade rotation occurs at 15 L/s with intermittent sticking. Progressive flow rate increases enhance both rotational speed and motion stability, culminating in stable 400 rpm operation at a flow rate of 30 L/s.

Simulation results demonstrate that the VCRT blade speed stabilizes at approximately 430 rpm in well Z401X, deviating by 7.50% from experimental data. The pressure drop measures 1.5 MPa, exhibiting a 6.25% deviation from experimental values. The discrepancy arises from the omission of internal friction effects within the VCRT in simulations, leading to deviations from actual conditions and quantifiable simulation errors. A detailed comparison is provided in Table 6.

### 4.2. Field application of VCRT

VCRT has been applied in 6 wells, including B9X, W18-7, and Z401X. From the on-site results, after applying VCRT, the friction in each well has decreased, and there has been a noticeable increase

**Table 5**Rotating blade rotation and flow field pressure drop under different flow rates.

Category	Drilling fluid flow rate, L/s	Rotation status of the rotating blades, rpm	Pressure difference at the inlet and outlet, MPa	Pressure drop in the flow field at the turbine structure, MPa
Experiment (with turbine-	15	Rotation with intermittent sticking	4.2	0.7
like structure)	20	Continuous rotation, with a speed of approximately 100	5.9	0.9
	25	Continuous rotation, with a speed of approximately 300	8.3	1.3
	30	Continuous rotation, with a speed of approximately 400	10.1	1.6
Experiment (non-turbine-	15		3.5	1
like structure)	20	1	5.0	1
ŕ	25	j	7.0	,
	30	Ī	8.5	1

### 4. Analysis of the practical application effect of VCRT

### 4.1. VCRT pressure drop and rotation speed testing

Before entering the wellbore, pressure drop and rotation speed tests are conducted indoors. Fig. 20(a) shows the VCRT stator, Fig.

Table 6
Comparison between simulation and experimental results.

	Pressure drop, MPa	Blade rotational speed, rpm
Simulation value Experimental value	1.5 1.6	430 400
Error	6.25%	7.50%

**Table 7**Changes in friction and torque after applying VCRT.

Well type Maximum well inclination		° Frictional resistance comparison			Torque comparison		
		Not using VCRT, kN	Using VCRT, kN	Comparative value, %	Not using VCRT, kN·m	Using VCRT, kN·m	Comparative value, %
в9Х	32.74	171.60	110.00	35.90	15.08	12.00	20.42
B9XC	43.77	188.90	120.00	36.47	15.86	11.00	30.64
W18-7	36.25	197.50	155.00	21.52	19.41	15.00	22.72
Z35-34	39.66	179.20	120.00	33.04	16.30	12.00	26.38
Z401X	38.98	312.00	200.00	35.90	23.22	16.00	31.09
C201X	41.71	347.70	220.00	36.73	26.27	18.00	31.48

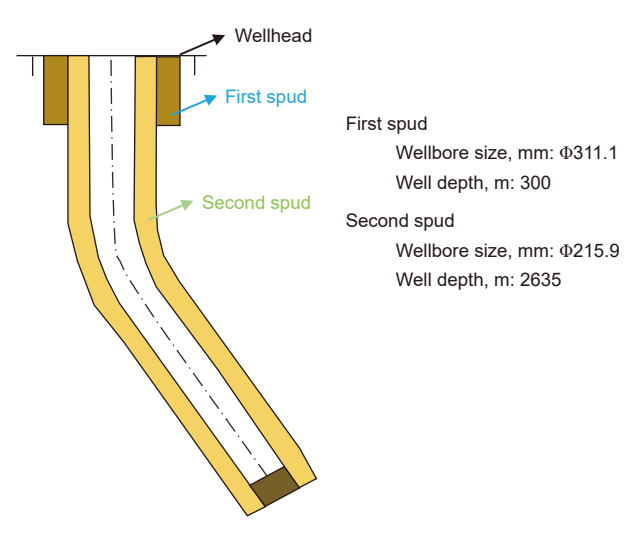


Fig. 22. Diagram of the wellbore structure of the deviated well Z401X

in the amount of cuttings collected at the surface. VCRT has achieved good results in reducing friction and removing cuttings in each well.

Table 7 presents friction and torque changes in wells B9X, W18-7, and Z401X after VCRT implementation. Friction losses and torque were reduced by over 20% in each well, with C201X exhibiting the most pronounced reductions of 36.73% and 31.48%, respectively.

An application analysis of VCRT in well Z401X has been conducted. This well has a total depth of 2635 m (vertical depth: 2325 m). The first hole section, with a 311.2 mm diameter, was



Fig. 23. The application of VCRT in well Z401X

**Table 8**Table of drilling parameters and friction resistance changes for different well depths of Z401X.

Well depth, m	Drilling pressure, kN	Flow rate, L/s	Density, kg/m <sup>3</sup>	Viscosity, Pa·s	Friction resistance, kN
1210	60/40	33	1150	0.043	40
1300	60/40	32	1150	0.044	40
1400	60/40	32	1150	0.043	50
1500	60/40	32	1170	0.045	60
1600	60/40	32	1170	0.045	70
1700	60/40	32	1170	0.047	80
1800	50/30	32	1170	0.045	100
1900	50/30	32	1200	0.045	120
2000	60/40	32	1200	0.045	120
2100	50/30	33	1200	0.046	130
2200	60/40	33	1200	0.047	140
2300	60/40	33	1200	0.044	160
2400	60/40	33	1200	0.044	170
2500	60/40	33	1200	0.044	180
2600	60/40	33	1200	0.044	190
2635	60/40	33	1200	0.044	200

**Table 9**Friction resistance variation within well Z401X.

Starting well section, m	Ending well section, m	,	Maximum wellbore deviation, °	Frictional resistance value without VCRT applied, kN	Frictional resistance value with VCRT applied, kN	Comparison, %
362	2447	2085	38.98	312.00	200.00	35.90

drilled to a depth of 300 m. Subsequent drilling extended the 215.9 mm diameter section to a total depth of 2635 m. Fig. 22 illustrates the deviated wellbore structure of well Z401X.

During the second drilling phase, the VCRT was installed 188 m behind the bit at a depth of 550 m during a short trip. The bit subsequently advanced from 550 m to 2635 m, yielding a total interval of 2085 m. The pure drilling time was 131.75 h throughout this operation, with an average rate of penetration (ROP) of 15.83 m/h. The VCRT functioned in a wellbore segment spanning 2085 m. Detailed depth-specific drilling parameters and friction variations are tabulated in Table 8, with operational configurations illustrated in Fig. 23.

During the drilling process in well Z401X, short trips usually proceed, and the wellbore inclination adjustment is smooth. The variation in friction resistance within well Z401X is illustrated in Table 9. The table shows that after applying VCRT, the frictional resistance at a drilling depth of 2635 m is 200 kN, compared to 312 kN without VCRT. The application of VCRT has reduced the frictional resistance by 35.90%, demonstrating significant effectiveness.

Field trials demonstrate a reduction in frictional resistance, confirming effective wellbore cleaning and significant annular pressure drop mitigation after using VCRT. This offset partially compensates for pressure losses generated by drilling fluid flow through the VCRT's internal channels. Therefore, the actual pressure drop resulting from using this tool can be considered negligible, indicating that pressure loss does not limit the quantities of the tool. Tool count is primarily dictated by field-specific cuttings removal requirements.

### 5. Conclusions

- (1) Based on the analysis of cuttings settling transport patterns and the modification of Moore's terminal settling velocity equation, a revised development of the annular cuttings transport model was established. The model specified VCRT placement 188 m from the bit, and when implemented in well Z401X, it achieved 35.90% friction reduction with superior cuttings clearance.
- (2) Numerical simulations comparing VCRT with conventional drilling tools revealed a 36.43% lower cuttings volume fraction along path 1 and threefold higher unit-time cuttings throughput at cross-section A under VCRT operation.
- (3) The numerical simulation results demonstrated that when the drilling fluid flow rate was 30 L/s, simulated results showed 430 rpm blade speed with 1.5 MPa pressure drop, whereas experimental data under identical conditions recorded 400 rpm and 1.6 MPa, demonstrating 7.50% and 6.25% deviations respectively.

Based on the specific drilling situation of the Z401 well, this article further studied the optimal installation position of cuttings removal tools within a turbine-like structure. The findings provide a reference for the precise installation of self-rotating tools, aiming to enhance the efficiency of cuttings.

### **CRediT authorship contribution statement**

Feng Chen: Software, Conceptualization, Writing – review & editing, Validation, Formal analysis, Methodology. Hong-Lin Lu: Software, Formal analysis, Writing – review & editing. Zhi-Hu Liu: Software, Formal analysis, Writing – original draft. Wen-Chang Wang: Conceptualization, Supervision, Project administration. Ya Liu: Project administration, Funding acquisition, Supervision. Wei Wang: Validation, Resources. Qin-Feng Di: Validation, Investigation.

### **Declaration of competing interest**

The authors declare that they have no known competing financial interests or personal relationships that could have appeared to influence the work reported in this paper.

### Acknowledgments

This research was supported by the National Natural Science Foundation of China (No. 52374008, No. 52174003) and Shanghai Leading Academic Discipline Project (No. S30106).

### References

- Andersen, L.B., 1998. Stochastic modelling for the analysis of blowout risk in exploration drilling. Reliab. Eng. Syst. Saf. 61 (2), 53–63. https://doi.org/10.1016/S0951-8320(97)00067-7.
- Boulet, J.G., Shepherd, J.A., Batham, J., Elliott, L.R., 2000. Improved hole cleaning and reduced rotary torque by new external profile on drilling equipment. SPE J. https://doi.org/10.2118/59143-MS.
- Chen, F., Liu, Z.H., Huo, Y.H., Liu, Y., Di, Q.F., Wang, W.C., 2022. Mechanical mechanism and removal effect of efficient vortexing cuttings removal tool. Adv. Mech. Eng. 14 (12), 1–14. https://doi.org/10.1177/16878132221143641.
- Han, X.Y., 2023. Simulation Analysis of Cuttings Migration in Extended Reach Borehole and Research of Directional Pulse Jet Tool. School of Mechanical Engineering Yangtze University (in Chinese). https://doi.org/10.26981/d.cnki. gibsc.2023.000288.
- Huang, L.P., 2002. Exploration of mechanical method for removing cuttings bed. Drill. Prod. Technol. 25 (3), 30–31, +4 (in Chinese). https://doi.org/10.3969/j. issn.1006-768X.2002.03.007.
- Jia, W.T., Yang, G.B., Song, L., Fu, J., 2023. Drilling speed-up technology of large displacement horizontal shale gas wells in North America. Int. Field Explor. Develop. Conf. 22 September 2023 (in Chinese). https://doi.org/10.26914/c. cnkihv.2023.059430.
- Khan, M.S., Barooah, A., Rahman, M.A., Hassan, I., Hassan, R., Maheshwari, P., 2021. Application of the electric resistance tomographic technique to investigate its efficacy in cuttings transport in horizontal drilling scenarios. J. Nat. Gas Sci. Eng. 95, 104119 (in Chinese). https://doi.org/10.1016/j.jngse.2021.104119.
- Li, Z.C., Yao, C.S., Hu, K.L., Lan, Z.Q., 2022. Research and practice of horizontal wellbore cleaning technology. Xinjiang Oil & Gas 18 (1), 48–53 (in Chinese). https://doi.org/10.3969/j.issn.1673-2677.2022.01.008.
- Liu, X.G., Fan, B.T., Yang, J., Cui, Z.J., Zhao, J., Li, C.L., Yue, W.K., Deng, H., 2016. Calculation spacing for cutting-bed-remover in highly deviated wells. Oil Field Equip. 45 (3), 46–50 (in Chinese). https://doi.org/10.3969/j.issn.1001-3482.2016.03.010.
- Mei, W.B., 2019. Application and development of large displacement technology in Bohai oilfield. China Petrol. Chem. Stand. Qual. 39 (10), 221–222 (in Chinese). https://doi.org/10.3969/j.issn.1673-4076.2019.10.107.
- Montes, A.C., Callerio, S., Turhan, Ç., Safarov, A., Ashok, P., Eric, V.O., 2024. Automatic determination of cuttings and cavings properties for hole cleaning and wellbore stability assessment using a laser-based sensor. SPE J. 29 (10), 5238–5257. https://doi.org/10.2118/217736-PA.

- Ozbayoglu, M.E., Saasen, A., Sorgun, M., Svanes, K., 2010. Critical fluid velocities for removing cuttings bed inside horizontal and deviated wells. Petrol. Sci. Technol. 28 (6), 594–602. https://doi.org/10.1080/10916460903070181.
- Pandya, S., Ahmed, R., Subhash, S., 2020. Wellbore cleanout in inclined and horizontal wellbores: the effects of flow rate, fluid rheology, and solids density. SPE Drill. Complet. 35 (1), 48–68. https://doi.org/10.2118/194240-PA.
- Pedrosa, C., Saasen, A., Ytrehus, J.D., 2023. Hole cleaning and wet-granular rheology of rock cutting beds: impact of drilling fluid composition. J. Petrol. Sci. Eng. 220, 111267. https://doi.org/10.1016/j.petrol.2022.111267.
- Qu, J.Y., 2021. Mechanical Model of Cuttings Transport and Evaluation of Hole Cleaning Effect in Horizontal Wells. Northeast Petroleum University (in Chinese). https://doi.org/10.26995/d.cnki.gdqsc.2021.000811.
- Qu, W.T., Zhou, D.P., Sun, C.M., 2017. Measures of cuttings removal and performance analysis of removing tool in complex structure well. Mech. Res. Appl. 30 (3), 99–101 (in Chinese). https://doi.org/10.16576/j.cnki.1007-4414.2017.03. 031
- Reinhardt, W.R., Williamson, R.N., Eaton, L.F., Actis, S.C., 2006. Magnolia deepwater development-striving for best-in-class drilling performance. SPE Drill. Complet. 21 (4), 268–278. https://doi.org/10.2118/92439-PA.
- Rodman, D., Wong, T., Chong, A., 2003. Steerable Hole Enlargement Technology in Complex 3D Directional Wells. SPE Asia Pacific Oil and Gas Conference and Exhibition, Jakarta, Indonesia, https://doi.org/10.2118/80476-MS.
- Sayindla, S., Lund, B., Ytrehus, J.D., Saasen, A., 2017. Hole-cleaning performance comparison of oil-based and water-based drilling fluids. J. Petrol. Sci. Eng. 159, 49–57. https://doi.org/10.1016/j.petrol.2017.08.069.
- Sun, K., 2023. Application of horizontal wellbore cleanness monitoring and evaluation while drilling. Drill. Eng. 50 (1), 102–106 (in Chinese). https://doi.org/10.12143/i.ztgc.2023.01.015.
- Van, P.L., Williams, H., 2013. Increasing Drilling Performance in ERD Wells with New Generation Drill Pipe. Unconventional Resources Technology Conference, Colorado, USA, 1229. https://doi.org/10.1190/urtec2013-108.

- Van, P.L., 2013. Increasing drilling performance using hydro-mechanical hole cleaning devices. SPE unconventional gas conference and exhibition. Muscat. https://doi.org/10.2118/164005-MS.
- Wang, J.J., Ge, B.H., Zou, C.M., 2013. Mechanism analysis and countermeasures of cuttings bed in large displacement horizontal wells. China Petrol. Chem. Stand. Qual. 33 (15), 138–139 (in Chinese). https://doi.org/10.3969/j.issn. 1673–4076.2013.15.130.
- Wylie, G., Zamora, F., Terry, J., Murali, B.N., 2002. Well Construction Efficiency Processes Yielding a Significant Step Change. SPE Annual Technical Conference and Exhibition, San Antonio, USA. https://doi.org/10.2118/77628-MS.
- Yu, Y., Fang, P., Zhang, B., He, Y.Y., Li, G., Xiao, D., 2023. Characteristics of cuttings migration with new cuttings removal device in horizontal well. Geoenergy Sci. Eng. 231, 212379. https://doi.org/10.1016/j.geoen.2023.212379.
- Zhang, X.C., Sun, L.P., Li, W.L., 2024. Dynamic cuttings transport law for shallow ultra-deep extended-reach wells in Bohai Sea. China Offshore Oil Gas 36 (4), 169–180 (in Chinese). https://doi.org/10.11935/j.issn.1673-1506.2024.04.
- Zhang, Y.C., Wang, J.J., Ju, S.D., Wang, X.T., 2017. Simulation and analysis of self-rotating cutting removing tool. China Petrol. Mach. 45 (9), 48–52 (in Chinese). https://doi.org/10.16082/j.cnki.issn.1001-4578.2017.09.009.
- Zhang, Y.Q., Hu, Z.W., Wu, X.Y., Liu, Y., Hu, X., Li, L.L., 2023. Study on structure optimization and cuttings removal efficiency of a vortex cuttings cleaner. SPE J. 28 (4), 1636–1649. https://doi.org/10.2118/214311-PA.
- Zheng, F., Wang, J.L., Wu, X.Y., Liu, X.S., Zhou, H.J., Xu, R.G., 2018. Analysis of cuttings bed in highly deviated well and application of new hole cleaning tool. Oil Field Equip. 47 (1), 80–82 (in Chinese). https://doi.org/10.3969/j. issn.1001-3482.2018.01.017.
- Zuo, H.G., He, F.Y., Yan, W.F., He, F.P., Zhang, Z.M., 2020. Research and engineering practice on wellbore cleaning technology for ultra deep and large displacement wells. Petrochem. Ind. Appl. 39 (2), 92–97 (in Chinese). https://doi.org/10.3969/j.issn.1673-5285.2020.02.021.